Defect and Diffusion Forum
ISSN: 1662-9507, Vol. 446, pp 13-19
doi:10.4028/p-9Zjg9v

Submitted: 2025-07-04
Accepted: 2025-10-23
Online: 2026-01-13

Modelling Combined Hardening Mechanisms in Alloys through the Analysis of Dislocation Percolation

Rafael Schouwenaars[1,2,a*]

[1]Departamento de Materiales y Manufactura, Facultad de Ingenieria, Edificio O, Universidad Nacional Autonoma de Mexico. Ciudad Universitaria, Coyoacan, 04510, Ciudad de Mexico, Mexico

[2]Ghent University, Materials Science and Technology, Department of Electromechanical, Systems and Metals Engineering, Technologiepark 46, 9052, Ghent, Belgium

[a]raf_schouwenaars@yahoo.com

Keywords: Micromechanics, Statistical modelling, Alloy strength, Strain hardening, Grain size effect.

Abstract. The critical resolved shear strength τ_{CRSS} of pure metals is given by the Peierls-Nabarro equation; impurities or alloying elements will significantly increase τ_{CRSS}. Additional strength is introduced by strain hardening (SH), the grain size effect (GSE), precipitates and particle dispersion. The combination of these mechanisms is generally described in an additive manner, which can be justified by the Taylor expansion of a multivariate function. This approach is highly empirical and involves extensive parameter fitting. The Kocks-Mecking model (KM) and discrete dislocation dynamics show that SH is mainly due to forest effects (latent hardening). Consequently, the main explanation for alloy strength must be sought in the resistance against dislocation percolation through a field of obstacles with different strengths, with the slip length limited by the grain diameter. This hypothesis is explored by reviving early graphical simulations to the percolation problem by introducing a grain boundary and variable obstacle strength in an efficient computer program. Such simulations and theoretical considerations demonstrate the limitations of the additive description of combined hardening. An alternative approximation is proposed, based on the statistical analysis of dislocation percolation, dislocation junctions and dislocation-grain boundary interaction.

Introduction

As noted by Cotrell [1,2], strain hardening was the first problem to be attempted by dislocation theory and may be the last to be solved. This statement refers to Taylor's first paper on dislocations [3], where he envisaged and equilibrium configuration consisting of a regular lattice of straight dislocation lines kept in place by their stress fields. Starting with the earliest direct observations of dislocations in alloys [4,5], it soon became clear that regular lattices were nowhere to be found, but the Taylor lattice was still considered as an explanation for strain hardening in the 1980s [6] and a large body of work on the statistical mechanics of dislocations is based on distributed densities of straight dislocations interacting through their stress fields [7-12].

Given the entangled nature of dislocation configurations found in deformed metallic materials, Saada [13], Schoek and Frydman [14] as well as Dupuy and Fivel [15] focused on the strength of dislocation junctions pinning dislocation sections as the main source of strain hardening. A first graphical attempt to analyse dislocation percolation through a field of stable dislocation junctions was presented by Kocks [16] and more extensive computer simulations of this process were made available in the 1990s [17,18], eventually leading to discrete dislocation dynamics software which accounts for both stress interaction and intersection between dislocations [19,20].

Combined hardening includes the effects of the lattice friction (Peierls stress τ_P), solid solution, grain size (d_g) and dislocation density (ρ_d). It is often approached by a simple superposition of effects, which can be justified as follows by considering an arbitrary, differentiable function of n variables, expanded in a Taylor series at the origin:

$$f(x_1, x_2, \ldots, x_n) \approx f(0) + \left.\frac{\partial \sigma_y}{\partial x_1}\right|_{\mathbf{x}=0} x_1 + \left.\frac{\partial \sigma_y}{\partial x_2}\right|_{\mathbf{x}=0} x_2 + \ldots + \left.\frac{\partial \sigma_y}{\partial x_n}\right|_{\mathbf{x}=0} x_n \quad (1)$$

then, for the yield strength in shear (τ_y) and setting $x_1 = \rho_d^{1/2}$, $x_2 = d_g^{-1/2}$ and $x_3 = X_{SS}^{1/2}$, with X_{SS} the atomic concentration of solutes, one finds:

$$\tau_y = \tau_P + \mu b \alpha \sqrt{\rho_d} + \frac{k_{HP}}{\sqrt{d_g}} + C_{SS}\sqrt{X_{SS}} \quad (2)$$

where μ is the shear modulus, α a constant with a value between 0.2 and 0.5 [2,21,22]. The term in $\rho_d^{1/2}$ is the classical Taylor equation [3] and can be rigorously proven either by dimensional analysis [23] or by an evolution equation for the dislocation density as a function of stress [24]. k_{HP} is the Hall-Petch constant and C_{SS} a constant which depends on the lattice misfit of the solute atom and the elastic properties of matrix and solute.

Similarly, the increase of dislocation density with the shear strain γ has been described as [25]:

$$\frac{d\rho_d}{d\gamma} = \frac{k_1\sqrt{\rho_d}}{b} - k_2\rho_d + \frac{k_3}{d_g} + \frac{k_4}{l_0} - \frac{1}{bs} + \frac{1}{2bd_t}\left(\frac{f_t}{1-f_t}\right) \quad (3)$$

The terms containing the fitting parameters k_1 and k_2 are the storage and annihilation terms of the original KM model. Using dimensional and statistical arguments, they can be rigorously proven [23,25,26]. Adding the term in k_3 defines the Kocks-Mecking-Estrin model; the addition of this term is purely empirical but justified by Eq. 1, as is the fifth term, which accounts for the spacing *s* between the sample surfaces (*b* is the magnitude of the Burgers vector). The sixth term introduces the effect of twins, with d_t the distance between the twins and f_t the twin fraction. To convert Eqs. (2) and (3) into expression for the yield strength and logarithmic strains in uniaxial tension, one writes $\sigma_y = M\tau_y$ and $\varepsilon = \gamma/M$, with *M* the average Taylor factor for the material.

The superposition of effects is widely accepted. It works because it represents a form of the Taylor expansion of a function of multiple variables. It does not present a method to calculate the values of the partial derivatives in Eq. (1), which must be fitted. Therefore, the approach is not predictive and Eqs. (2) and (3) require extensive experimentation to determine these parameters. By adding more parameters, better fits can always be obtained but predictivity is lost. Extrapolation to ranges which are not covered by experiments is risky.

This short paper will explore the existing theoretical calculations which provide an alternative, physics-based approach for simple superposition [23,24,27]. The essential difference between weak and strong obstacles will be explained and their effects explored by some simple simulations. The strong obstacles are accounted for by the theory; weak obstacles can be lumped together in a friction term, but their quantitative analysis, based on arguments of stochastic geometry, must be studied into more detail in future work.

Theoretical Results

The behaviour of a dislocation which is pinned in the slip plane by a row of obstacles is shown in Fig. 1. A general expression for the line tension of a dislocation is given by:

$$S = \frac{\mu b^2}{4\pi}\left(\cos^2\psi + \frac{\sin^2\psi}{1-\nu}\right)\ln\frac{R}{r_0} \approx \alpha_0 \mu b^2 \quad (4)$$

where ψ is the angle between the dislocation line and the Burgers vector, *R* is an upper cut-off radius and r_0 a lower cut-off. *R* is an artifact caused by considering infinite dislocation lines, it does not appear when closed dislocation loops are considered [28,29]. r_0 is closely connected to the width of the dislocation core. The second equality lumps all geometrical constants in a single parameter α_0, defining the isotropic line tension approach. It shall be noted that α_0 is not equal to α in Eq. (2) [24]. Under this assumption [13,16], the dislocation segment will bow out between the obstacles in the form of a circular arc with radius r_τ under the effect of a resolved shear stress τ:

$$r_\tau = \frac{\alpha_0 \mu b^2}{2\tau} \tag{5}$$

The force on an obstacle is given by:

$$F = S\sin\theta_1 + S\sin\theta_2 = \mu b^2 \alpha_0 (\sin\theta_1 + \sin\theta_2) = \frac{(s_1+s_2)\tau}{\mu b \alpha_0} \tag{6}$$

The value of $\sin\theta \leq 1$. If the obstacle fails before $\sin\theta = 1$, it is called a weak obstacle. Weak dislocation junctions will unzip [13-15]. Weak precipitates will be cut. If $\sin\theta = 1$, the moving dislocation will bow-out, remaining pinned on the original obstacle. This corresponds to the Orowan-mechanism for dispersion hardening.

Once a weak obstacle is passed, it no longer affects the length of the stored dislocations but the energy stored in the pinned configuration is liberated and dissipates in the form of phonons [30]. The corresponding transformation of mechanical energy into heat is a friction phenomenon. Strong obstacles modify the length distribution of the stored dislocations. The density of solute atoms, precipitates and particles (including non-shearable precipitates) is constant; the density of weak and strong dislocation junctions increases during strain hardening.

If the spatial distribution of the obstacles is defined by a Poisson point process, the length distribution of the dislocation segments can be addressed by closed-form calculations [24]. Considering that, at a given stress τ, no segment can be longer than $s_\tau = 2r_\tau$, it can be written that the number of dislocation segments released upon an increase of τ is [24]:

$$dn = -\frac{\rho_s}{\langle s \rangle} p_S(s_\tau|\tau) ds_\tau \tag{7}$$

ρ_s is the dislocation density in each of the slip planes, which can be proven to be proportional to the amount of slip in this plane. $\langle s \rangle$ is the average segment length and $p_S(s_\tau|\tau)$ is the probability density of the segment lengths at a given value of τ. Each bow-out event causes a sequence of new bow-outs which can be analysed by classical probability calculus [24]. The result is:

$$\frac{d\rho_d}{d\tau} = \frac{\mu b \alpha_0}{\tau^2} \sqrt{\varphi_c} \rho_d^{3/2} K\left(\frac{\mu b \alpha_0}{\tau} \sqrt{\varphi_c \rho_d}\right) \tag{8}$$

The full form of $K(\cdot)$ takes a complete page and is given in the appendix of Ref. [24]; φ_c is the fraction of the dislocations that can form stable junctions with the dislocations in the slip system. It was proven that the Taylor equation $\tau_y = \mu b \alpha \sqrt{\rho_d}$ solves this equation and that this solution is unique [23]. Non-shearable precipitates, with an effective slip plane density ρ_p, modify the evolution as:

$$\frac{d\rho_d}{d\tau} = \frac{\mu b \alpha_0}{\tau^2} \rho_d^{3/2} \sqrt{\varphi_c + \frac{\rho_p}{\rho_d}} K\left(\frac{\mu b \alpha_0}{\tau} \sqrt{\varphi_c \rho_d + \rho_p}\right) \tag{9}$$

The grain size effect can be accounted for by making a balance between the dislocations originating at the grain boundaries (GBs) and in the substructure and the ones absorbed by the GBs or stored/annihilated in the substructure [27]. Under the assumption that the storage and annihilation sites define independent Poisson point processes along the dislocation path, it was shown that:

$$\frac{d\rho_d}{d\gamma} = \frac{1}{b\langle\lambda\rangle}\left(\frac{k_1\sqrt{\varphi_c\rho_d} - k_2 b \varphi_s \rho_d}{k_1\sqrt{\varphi_c\rho_d} + k_2 b \varphi_s \rho_d}\right) \tag{10}$$

where $\langle\lambda\rangle$, the expected value of the slip length in presence of GBs, can be obtained by probability calculus [27]. It was found that:

$$\langle\lambda\rangle = \frac{d_g\left(k_1\sqrt{\varphi_c\rho_d} + k_2 b \varphi_s \rho_d\right)}{d_g + k_1\sqrt{\varphi_c\rho_d} + k_2 b \varphi_s \rho_d} \tag{11}$$

The result is slightly generalised as compared to ref. [27], in the sense that in both the storage term and the annihilation term, the fraction of the dislocations crossing the slip plane (φ_c) and the fraction inside the slip plane (φ_s) are considered. Notice that $\varphi_s \neq 1 - \varphi_c$, because not all combinations of slip systems produce stable dislocation junctions [15,19].

With Eq. (9), the Taylor equation is no longer an exact solution. A numerical solution still provides a relationship between ρ_d and τ. Under the assumption that precipitates are randomly and independently distributed in the slip plane, Eqs. (10) and (11) can be recombined as:

$$\frac{d\rho_d}{d\gamma} = k_1 \frac{\sqrt{\varphi_c \rho_d + \rho_p}}{b} - k_2 \varphi_s \rho_d + \frac{1}{b d_g} \left(\frac{k_1 \sqrt{\varphi_c \rho_d + \rho_p} - k_2 b \varphi_s \rho_d}{k_1 \sqrt{\varphi_c \rho_d + \rho_p} + k_2 b \varphi_s \rho_d} \right) \tag{12}$$

Eqs. (9) and (12) provide a set of two non-linear ordinary differential equations describing the evolution of the dislocation density on each slip system. While φ_s and φ_d are proportional to the activity of the slip systems as found from crystal plasticity models in the case of pure strain hardening, here it follows that less-active slip systems will have a higher strain hardening rate, as φ_s is lower and φ_c higher. Consequently, the set of equations must be solved for all slip systems simultaneously.

Simulations

To explore the relative importance of weak vs. strong obstacles, a software package was developed in which, after bow-out or unzipping, the dislocation samples the next closest obstacle to expand through the random field of points. This field is delimited by a circle of impenetrable obstacles defining the GB. The dislocation density is the inverse of the number of points n_p in the Poisson process and value of r_τ defines the stress through Eq. (5). A higher value of n_p corresponds to a higher dislocation density or a larger grain size. The goal of these simulations is to gain an insight into the role of weak obstacles. To do so, their fraction is defined as f_w and their strength, defined as $sin\,\theta$, follows a uniform distribution on [0,1]. Examples for $f_w = 0$ and 1 are given in Fig. 1.

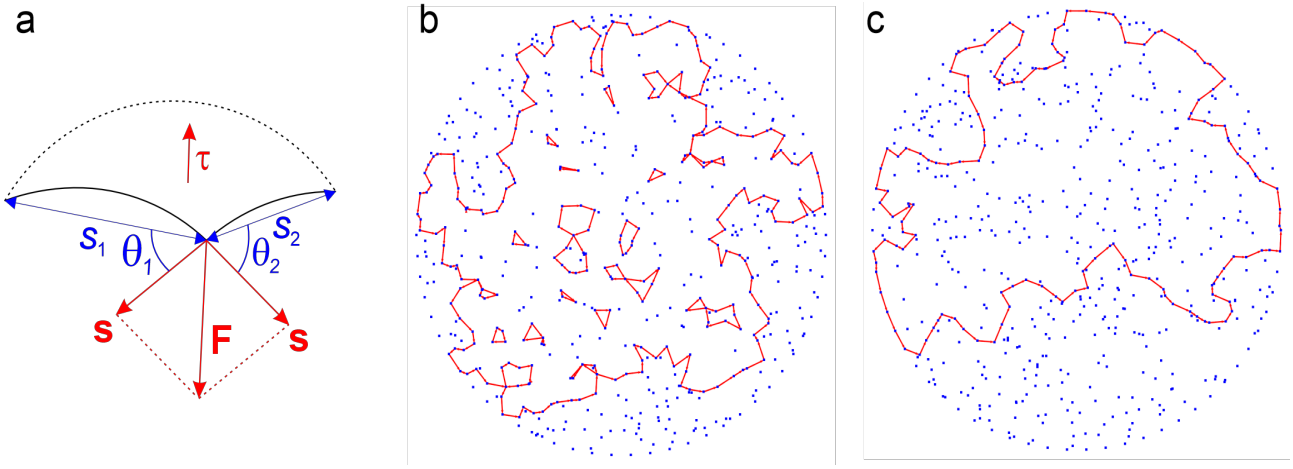

Fig. 1. a) Geometry showing two circular dislocation segments blocked by a weak obstacle. The force on the obstacle is equal to the sum of the line tension vectors. Cutting of the obstacle will allow the dislocation to expand to the dashed configuration. b) Example of the percolation of a dislocation loop in a field of strong obstacles. c) With weak obstacles, the stored dislocation length is lower.

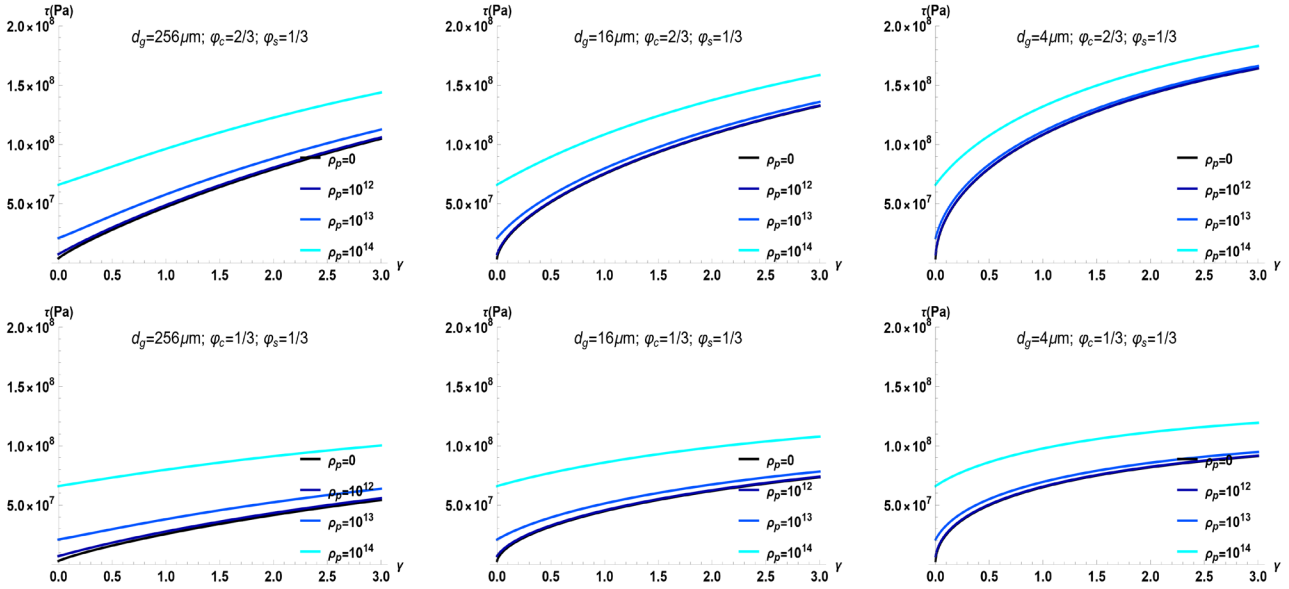

Fig. 2. Examples of $\tau - \gamma$ curves for different grain sizes and particle densities.

To test the result of Eqs. (9) and (12), a fixed value of $\varphi_s = 1/3$ is used and $\varphi_c = 2/3$ and 1/3 are tested, corresponding to three slip systems with equal activity and 100% and 50% strong junctions. No lattice friction is considered, which means that weak obstacles are not included in the analysis. The results show that the strain hardening rate is higher in small grains and that particle strengthening is less pronounced, clearly illustrating that strengthening effects are not additive.

Conclusions

A brief review was provided on the development of the concept of statistical micromechanics to describe the combined effects of hardening mechanisms in metals and alloys. An essential distinction must be made between strong and weak obstacles, with the latter contributing to the lattice friction and the former collectively contributing to strain hardening, in a non-additive manner. The theoretical analysis of strong obstacles and grain boundaries leads to a set of ordinary differential equations which produce realistic stress-strain curves and naturally including multi-slip in crystal plasticity. To eliminate the empirical approximation to lattice friction, the study of weak obstacles must be refined.

Acknowledgements

This research was sponsored by DGAPA grant IN113123.

References

[1] Cottrell AH. Dislocations and plastic flow in crystals. Oxford: Oxford University Press; 1953.

[2] Kocks, U.F., Mecking, H. Physics and phenomenology of strain hardening: the FCC case. Prog. Mater. Sci. 48 (2003) 171-273.

[3] Taylor, G.I. The mechanism of plastic deformation of crystals. Part I.—Theoretical. Proc. Roy. Soc. A, 145 (1934) 362-387.

[4] Wilsdorf, H., Kuhlmann-Wilsdorf, D. Direct evidence for dislocations in aluminium-copper alloys. Lond. Edinb. Dubl. Phil. Mag. 45 (1954) 1096-1097.

[5] Hirsch, P.B., Horne, R.W., Whelan, M.J. Direct observations of the arrangement and motion of dislocations in aluminium. Phil. Mag. 86 (1956) 677-684.

[6] Kuhlmann-Wilsdorf, D. Theory of plastic deformation:-properties of low energy dislocation structures. Mater. Sci. Eng. A. 113 (1989) 1-41.

[7] Zaiser, M., Miguel, M.C. Groma, I. Statistical dynamics of dislocation systems: The influence of dislocation-dislocation correlations. Phys. Rev. B, 64 (2001) 224102.

[8] Yefimov, S., Groma, I., Van der Giessen, E. A comparison of a statistical-mechanics based plasticity model with discrete dislocation plasticity calculations. J. Mech. Phys. Sol. 52 (2004) 279-300.

[9] Ananthakrishna, G. Current theoretical approaches to collective behavior of dislocations. Phys. Rep. 440 (2007) 113-259.

[10] Hochrainer, T. Multipole expansion of continuum dislocations dynamics in terms of alignment tensors. Phil. Mag. 95 (2015) 1321-1367.

[11] Ispánovity, P.D., Laurson, L., Zaiser, M., Groma, I., Zapperi, S. Alava, M.J. Avalanches in 2d dislocation systems: Plastic yielding is not depinning. Phys. Rev Lett. 112 (2014) 235501.

[12] Zhang, Y., Wu, R. Zaiser, M. Continuum dislocation dynamics as a phase field theory with conserved order parameters: formulation and application to dislocation patterning. Mod. Sim. Mater. Sci. Eng. 33 (2025) 035011.

[13] Saada, G. Sur le durcissement dû à la recombinaison des dislocations. Acta Metall. 8 (1960) 841-847.

[14] Schoeck, G., Frydman, R. The contribution of the dislocation forest to the flow stress. Phys. Stat. Sol. B. 53 (1972) 661-673.

[15] Dupuy, L., Fivel, M.C. A study of dislocation junctions in FCC metals by an orientation dependent line tension model. Acta Mater. 50 (2002) 4873-4885.

[16] Kocks, U.F. A statistical theory of flow stress and work-hardening. Phil. Mag. A. 13 (1966) 541-566.

[17] Hernández Olivares, F., Gil Sevillano, J. A quantitative assessment of forest-hardening in FCC metals. Acta Metall. 35 (1987) 631-641.

[18] Gil Sevillano, J., Bouchaud, E., Kubin, L. P. The fractal nature of gliding dislocation lines. Scripta Metall. Mater. 25 (1991) 355-360.

[19] Devincre, B., Hoc, T., Kubin, L. Dislocation mean free paths and strain hardening of crystals. Science, 320 (2008) 1745-1748.

[20] Lu, S., Kan, Q., Zaiser, M., Li, Z., Kang, G., Zhang, X. Size-dependent yield stress in ultrafine-grained polycrystals: A multiscale discrete dislocation dynamics study. Int. J. Plast. 149 (2022) 103183

[21] Hansen, N., Huang, X., Microstructure and flow stress of polycrystals and single crystals. Acta Mater. 46 (1998) 1827-1836

[22] Gil-Sevillano, J. Flow stress and work hardening. Materials science and technology, Wiley, 2006.

[23] Schouwenaars, R. Some basic results in the mathematical analysis of dislocation storage and annihilation in stage II and stage III strain hardening. Phil. Mag. A. 94 (2014) 3120-3136.

[24] Schouwenaars, R. A statistical analysis of strain hardening: The percolation limit and the Taylor equation. Acta Mater. 60 (2012) 6331-6340.

[25] Joshi, S.S., Keller, C., Mas, L., Lefebvre, W., Hug, E., Couzinie, J.P. On the origin of the strain hardening mechanisms of Ni20Cr alloy manufactured by laser powder bed fusion. Int. J. Plast. 165 (2023) 103610.

[26] Essmann, U., Mughrabi, H. Annihilation of dislocations during tensile and cyclic deformation and limits of dislocation densities. Phil. Mag. A. 40 (1979) 731-756.

[27] Schouwenaars, R. Calculating the grain size effect during strain hardening through a probabilistic analysis of the mean slip distance in polycrystals. Int. J. Plast. 178 (2024) 104012.

[28] Schouwenaars, R. 2020. Self-energy, line tension and bow-out of grain boundary dislocation sources. Int. J. Plast. 133, 102802

[29] Schouwenaars, R., Kestens, L.A.I., 2023. Dislocation pileups in small grains. Int. J. Plast. 164, 103602.

[30] Kubin, L., 2013. Dislocations, mesoscale simulations and plastic flow. Oxford University Press.

The publication of this article was funded by the Universidad Nacional Autónoma de México 10.13039/501100005739